High-resolution deconvolution applied to non destructive testing

Ewen Carcreff, Sébastien Bourguignon, Jérôme Idier, Laurent Simon

ACOUSTICS 2012

High-resolution deconvolution applied to non destructive testing

E. Carcreff[a,b], S. Bourguignon[b], J. Idier[b] and L. Simon[a]

[a]Laboratoire d'acoustique de l'université du Maine, Bât. IAM - UFR Sciences Avenue Olivier Messiaen 72085 Le Mans Cedex 9

[b]IRCCyN, Ecole centrale de Nantes, 1 rue de la Noë, 44321 Nantes, France

ewen.carcreff@irccyn.ec-nantes.fr

Ultrasonic non destructive testing consists in emitting an acoustic wave in a material and then locating the reflected echoes produced by impedance changes, due to flaws or medium discontinuities. In some cases, echoes can overlap in the A-scan (typically for layered materials), yielding a difficult analysis: techniques such as matched filtering may fail and advanced techniques are necessary to locate the echoes. Sparse deconvolution methods have been recently applied to such problems. The challenge is to estimate a sparse sequence describing the echoes locations (times of flight) and amplitudes. Usually, deconvolution is addressed by restoring a discrete signal at the sampling period of the data. This limits the precision of the spike location and may cause spike splitting. In this paper, we consider a super-resolution formulation of the deconvolution problem with a more precise restoration grid. To do so, we extend a recently proposed approach which minimises a data misfit least-square criterion, penalised by a L_0-norm term. The method is evaluated on synthetic data, revealing possible improvements in the estimation of times of flight.

1 Introduction

Nondestructive testing (NDT) aims at locating flaws and characterising the geometry in materials. The standard procedure uses an ultrasonic probe in a pulse-echo mode thanks to high impedance contrasts in industrial parts [1]. The electronic system sends a short pulse to the transducer that generates an acoustic motion in the material. The wave propagates then in the material, creating an echo at each impedance change. The signal received by the transducer (the *A-scan*) is finally the superposition of all echoes. If the reflectors are point targets and if no diffraction is considered, a convolution model can be formulated [2]. When the echoes are clearly separate, a diagnostic by eye can easily be obtained or the well-known *matched filter* can be employed. For more difficult cases (close flaws, multi-layered materials, *etc.*), echoes may overlap and advanced techniques are required to separate the contributions of each echo. The goal is then to restore, by deconvolution, a sparse sequence (called reflectivity sequence) that locates the material discontinuities. Usually, such a sequence is estimated at the data sampling frequency, limited by the electronic system [3, 4]. This paper studies the possibility of increasing the location precision by a super-resolution (SR) approach.

Deconvolution techniques have been studied for NDT purposes, where the solution is defined as the minimiser of a composite criterion, composed of a data fitting term and a penalisation term [3, 4, 5]. The penalisation strengthens the sparse nature of the solution. In the literature cited above, a L_1-norm is usually used. Recently, L_0-penalisation has been studied for sparse deconvolution [8]. Here, we consider the extension of these works to the super-resolution formulation.

The paper is organised as follows. In Section 2, we build the super-resolution discrete model based on the description of the physical model. Then, Section 3 extends the Single Best Replacement algorithm introduced in [8] to perform SR deconvolution. Section 4 presents simulation results with a simple example and NDT-like synthetic data. Finally, conclusions and perspectives are addressed in Section 5.

2 Signal Model

2.1 Physical model

The pulse-echo signal received by the transducer may be considered as the sum of the echoes coming from the point scatterers [2]. The output voltage $y(t)$ depends on the electric excitation $u(t)$ through a set of transfer functions. If we do not consider any diffraction effect, no flaw signature and no frequency-dependent attenuation, the signal received by the transducer reads [6] :

$$y(t) = u(t) * h_{ea}(t) * x(t) * h_{ae}(t), \tag{1}$$

where $h_{ea}(t)$ and $h_{ae}(t)$ are respectively the electro-acoustical and acousto-electrical responses of the transducer. The signal $x(t)$ is a sparse reflection sequence that describes the material inhomogeneities [6], which synthesises the coherent summation of the echoes. If we consider a set of reflectors indexed by i, the reflectivity sequence is composed of the times of flight t_i such that :

$$x(t) = \sum_i a_i \delta(t - t_i), \tag{2}$$

where a_i is the amplitude of the i-th echo that models the frequency-independent attenuation or the reflective coefficient of a flaw. Sequence $x(t)$ has a spatial interpretation :

$$R(r) = \sum_i a_i \delta(\boldsymbol{r} - \boldsymbol{r}_i), \tag{3}$$

where $\boldsymbol{r}$ is the vector of coordinates of any point of the space and $\boldsymbol{r}_i$ are the positions of the reflectors. $R(\boldsymbol{r})$ is the scalar reflectivity at position $\boldsymbol{r}$ having non-zero values at $\boldsymbol{r}_i$. If the speed of sound c is constant (*i.e.*, if a uniform material is considered), $\boldsymbol{r}_i$ is the distance corresponding to the time of flight t_i such as $|\boldsymbol{r}_i| = t_i c/2$.

For clarity purposes, we consider $h(t) = u(t) * h_{ea}(t) * h_{ae}(t)$ as the transducer impulse response since it is the response of a point target depending only on the transducer properties. From Eq. (1) and due to the properties of the convolution operation, the direct model can be formulated by :

$$y(t) = (h * x)(t) = \int_{-\infty}^{+\infty} h(\tau)\, x(t - \tau) \mathrm{d}\tau. \tag{4}$$

In this paper, we suppose that $h(t)$ is known. To obtain this response experimentally, it is possible to measure the echo-field on a rigid wall placed in the far field in order to minimise the diffraction effects. The problem is that the signal-to-noise ratio is weak at this distance [6]. Another method, based on a similar measurement but in the near field, is to deconvolve the received signal from the corresponding *radiation coupling function* [7].

2.2 Discrete model

In practice, available data take a discrete form, which corresponds to sampling $y(t)$ in Eq. (4). If T_S is the sampling period, y_n is the discrete-time signal corresponding to the continuous signal $y(t)$ such that $y_n = y(nT_S)$. Numerical methods

then usually consider a discretised version of the right-hand term in Eq. (4), at the sampling period T_S of y_n. It leads consequently to the well-known discrete convolution model:

$$y_n = \sum_{m=0}^{M-1} h_m \, x_{n-m} + e_n. \tag{5}$$

where $h_m = h(mT_S)$. We introduce here an error term e_n which describes the perturbations, the sampling errors and the model errors (in particular, diffraction, frequency-dependent attenuation, flaw signatures are not considered). For the sake of convenience, the discrete signals y_n, h_n, x_n and e_n are respectively concatenated to build column vectors $\boldsymbol{y}$, $\boldsymbol{h}$, $\boldsymbol{x}$ and $\boldsymbol{e}$. Eq. (5) then reads:

$$\boldsymbol{y} = \mathbf{H}\boldsymbol{x} + \boldsymbol{e}, \tag{6}$$

where $\mathbf{H}$ is a convolution matrix whose lines are delayed versions of the reversed discrete wavelet $\boldsymbol{h}^T$ or, equivalently, whose columns are delayed versions of $\boldsymbol{h}$.

Note that this formulation, where the discretisation of the convolution model is considered at the sampling frequency, appears in all deconvolution problems in NDT up to our knowledge [3, 4]. The contribution of this paper is precisely to consider a finer discretisation of the convolution terms in Eq. (4). This seems coherent since the reflectivity sequence $x(t)$ is sparse and hence has high frequency components. Let us consider that $h(t)$ and $x(t)$ are discretised at T_S/K with K integer. The discrete convolution model in Eq. (5) becomes:

$$y_n = \sum_{p=0}^{P-1} h^{sr}_p \, x^{sr}_{nK-p} + e_n, \tag{7}$$

where n is the index of the data samples and p is the index for the super-resolution restored signal. One then has $P = KM$ and $h^{sr}_p = h(pT_S/K)$, where $h(t)$ is the continuous-time wavelet in Eq. (4). Compared to the data y_n, the sampling period of h^{sr}_n and x^{sr}_n is now divided by K. In practice, since h is measured at the sampling rate of the data, the original discrete wavelet has to be up-sampled by factor K to form h^{sr}. This can be done by time interpolation. From the model in Eq. (7), the sequence x^{sr} will be restored at super-resolution rate T_S/K, increasing K times the precision. With $\boldsymbol{h}^{sr}$ and $\boldsymbol{x}^{sr}$ the super-resolution versions of $\boldsymbol{h}$ and $\boldsymbol{x}$, the problem can be written in matrix form:

$$\boldsymbol{y} = \mathbf{H}^{sr}\,\boldsymbol{x}^{sr} + \boldsymbol{e}, \tag{8}$$

where each line of $\mathbf{H}^{sr}$ is formed by the reversed wavelet $\left[h^{sr}_{P-1} \dots h^{sr}_0\right]$ with nK zeros inserted at the beginning. An example is given for $K = 2$:

$$\mathbf{H}^{sr} = \begin{bmatrix} h^{sr}_{P-1} & \cdots & \cdots & h^{sr}_0 & 0 & 0 & 0 & 0 & \cdots \\ 0 & 0 & h^{sr}_{P-1} & \cdots & \cdots & h^{sr}_0 & 0 & 0 & \cdots \\ 0 & 0 & 0 & 0 & h^{sr}_{P-1} & \cdots & \cdots & h^{sr}_0 & \cdots \\ 0 & 0 & 0 & 0 & 0 & 0 & h^{sr}_{P-1} & \cdots & \cdots \\ \vdots & & & & & & & & \ddots \end{bmatrix}. \tag{9}$$

This matrix corresponds to K interleaved convolution matrices. Equivalently, the model can be written as the sum of K discrete convolutions as :

$$y_n = \sum_{k=0}^{K-1} \left(\sum_{m=0}^{M-1} h^k_m \, x^k_{n-m} \right) + e_n, \tag{10}$$

where $h^k, k = 0 \dots K-1$ are K *sub-wavelets* with sampling period T_S, such that $h^k_m = h(kT_S/K + mT_S)$ and $x^k, k = 0 \dots K-1$ are the corresponding sparse sub-sequences with M points. The decomposition in matrix form hence gives :

$$\boldsymbol{y} = \sum_{k=0}^{K-1} \mathbf{H}^k \, \boldsymbol{x}^k + \boldsymbol{e}, \tag{11}$$

with $\mathbf{H}^k$ the *sub-matrices* obtained by taking every K columns of $\mathbf{H}^{sr}$. The pulse-echo signal can therefore be modelled as a *super-resolution convolution* written in Eq. (8) (which is not a discrete convolution), or equivalently as the superposition of K discrete convolutions in Eq. (11).

3 The Super-Resolution deconvolution algorithm

According to Eq. (6), the goal of deconvolution is to find a solution $\boldsymbol{x}$ knowing the data $\boldsymbol{y}$ and matrix $\mathbf{H}$ (or wavelet $\boldsymbol{h}$). Deconvolution of ultrasonic pulse echoes is an ill-posed problem especially because the solution is unstable in the presence of noise: the best least-squares fit leads in particular to unacceptable noise amplification [5]. Moreover, in the SR formulation, the solution is not unique since the number of unknowns is (K times) larger than the number of data. In order to overcome such difficulties, it is necessary to use regularised methods. A well-known method is the minimisation of a penalised least-square criterion. For the problem in Eq. (6), such a criterion reads:

$$J(\boldsymbol{x}, \mu) = \|\boldsymbol{y} - \mathbf{H}\,\boldsymbol{x}\|^2 + \mu\phi(\boldsymbol{x}), \tag{12}$$

where $\mu > 0$ manages the trade-off between data fitting and regularisation. The solution $\hat{\boldsymbol{x}}$ is then defined as the minimiser of $J(\boldsymbol{x}, \mu)$. In the context of sparse deconvolution, regularisation aims to favour zero values in $\hat{\boldsymbol{x}}$. Many contributions to sparse deconvolution in NDT choose ϕ as a L_1-norm (for example, [3, 4]). The convexity of this norm and the resulting criterion J leads to efficient optimisation strategies.

In this paper, we follow [8] and handle L_0 regularisation where the L_0-pseudo-norm $\|\boldsymbol{x}\|_0$ is the number of non-zero elements in $\boldsymbol{x}$. The data misfit criterion hence becomes in a super-resolution approach:

$$J(\boldsymbol{x}^{sr}, \mu) = \|\boldsymbol{y} - \mathbf{H}^{sr}\,\boldsymbol{x}^{sr}\|^2 + \mu\,\|\boldsymbol{x}^{sr}\|_0\,. \tag{13}$$

Optimisation is more complex for this norm because it is mainly a combinatorial problem. The number of possible combinations can be very large and it is numerically intractable to test all the combinations. The algorithm used here is the Single Best Replacement (SBR) algorithm [8]. It is an iterative algorithm that starts from a zero-signal and gradually adds or removes elements one by one, selecting the replacement that most decreases the criterion. Although such strategy is not theoretically ensured to converge to the global minimum of (13), satisfactory results were obtained for sparse deconvolution at "normal" resolution, outperforming other usual sparsity-based algorithms and the L_1-penalisation approach, especially at high SNR [11].

Initial works introducing the SBR algorithm proposed a generic implementation, where matrix $\mathbf{H}$ is not necessarily a convolution matrix. For low dimension problems, it is possible to build the matrix $\mathbf{H}^{sr}$ in Eq. (8) and use this generic

version. On the other hand, for large problems, it is no more possible to store matrix $\mathbf{H}^{sr}$. Therefore, we have developed a specific implementation based on the formulation in Eq. (11) that only requires to store the K *sub-wavelets* $\boldsymbol{h}^k$.

Tuning parameter μ in Eq. (13) is crucial, since it controls the sparsity degree, that is, the number of spikes, in the solution. Let $\boldsymbol{z} = \mathbf{H}^{sr\,T}\boldsymbol{y}$ and note $\boldsymbol{h}_k^{sr}$ the k-th column of matrix H^{sr}. It can be shown that for $\mu > \mu_{\max}$ with $\mu_{\max} = \max_k z_k^2 / \left\|\boldsymbol{h}_k^{sr}\right\|^2$, the solution is identically zero. A *continuation* version of SBR was proposed in [9], which enables one to compute the set of minimisers obtained for all $\mu \in [\mu_{\min}, \mu_{\max}]$, for few additional cost compared to the solution obtained for $\mu_{\min}$. Optimal parameter μ can then be estimated from all solutions by informational criteria such as Minimum Description Length or Akaike's Information criterion [10].

4 Application to synthetic examples

This section presents the results of standard and super-resolution deconvolution applied to synthetic data. For the sake of clarity, we call Data-Resolution (DR) the resolution of the data. In the first example, the problem of time of flight estimation of a single echo is treated. Secondly, we will apply deconvolution with the SBR algorithm to a synthetic A-scan signal from a thin plate. Lastly, we study the case of two close flaws provoking strongly overlapping echoes.

4.1 Time of flight estimation of a single echo

The wavelet $h(t)$ is simulated as a sine wave with a Gaussian envelope. The wavelet is then time-shifted by a delay t_0 so that the signal received by the transducer is :

$$y(t) = h(t - t_0). \tag{14}$$

The goal is then to estimate the time delay t_0. The central frequency of the transducer is 5 MHz and the sampling frequency of the electronic system is 50 MHz ($T_S = 20$ ns). The up-sampling parameter is $K = 4$, meaning that the SR sampling frequency is 200 MHz (*i.e.* a time resolution of 5 ns). In this toy example, the deconvolution process is needless since only one spike is searched. Therefore, the result is identical to a *matched-filter* or *cross-correlation* operation.

In Figure 1, results of both DR and SR processing are presented for two values of time-shift : $t_0 = 2010$ ns and $t_0 = 2012$ ns. The first value belongs to the SR discretisation grid whereas the second does not. Both values of t_0 do not belong to the DR grid. We consider noise-free data and 10 dB noise corrupted data, where the Signal-to-Noise Ratio (SNR) is defined as the ratio between the power of $\boldsymbol{x} * \boldsymbol{h}$ over the power of noise $\boldsymbol{e}$. One can notice that, when t_0 fits the SR grid, the result of SR estimation obviously gives the exact solution. Concerning the DR approach, it returns the closest sampling time, yielding an error of estimation that can reach $T_S/2$. In the same sense, if t_0 is not on any restoration grid, the time estimation is the closest time reference, giving advantage to the SR approach, since the maximum error is then $T_S/2K$. Similar results are achieved with noise-corrupted data. Nevertheless, the estimated location of t_0 may vary, depending on the noise random realisation. It is accordingly interesting to observe the time-of-flight estimation distribution obtained for a large number of noise realisations.

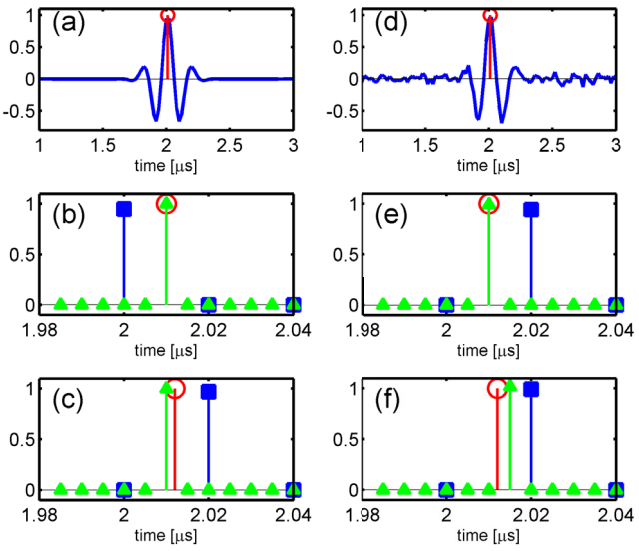

Figure 1: Results of time of flight estimation for a single echo. Left: noise-free case, right: SNR = 10 dB. Top: data, centre: $t_0 = 2010$ ns, bottom: $t_0 = 2012$ ns. Truth (○), estimation at DR (□) and estimation at SR with $K = 4$ (△).

Monte-Carlo runs enable to test this at a given SNR. Figure 2 reveals the distribution of time of flight estimations using DR and SR deconvolution for SNR = 0 dB. We can observe that the distribution of the spike location estimated at DR spreads over two values, on both sides of the true time delay. Such error can reach half the sampling frequency. On the other hand, for SR deconvolution, the distribution shows less dispersion around the true delay. We note that such dispersion is of the same order of magnitude as the minimum variance obtained for typical time delay estimation (TDE) problems. For example, in [12], the minimum variance on the TDE is approximated by:

$$\sigma^2 \geq \frac{3}{8\pi^2 T}\frac{1}{\mathrm{SNR}}\frac{1}{f_2^3 - f_1^3}, \tag{15}$$

where T is the observation time, f_1 and f_2 are the lower and higher bounds of the signal bandwidth. In our example, the empirical standard deviation in Figure 2 is coherent with such theory. In practice, this may give a guideline in order to select the value of the SR factor K: it is indeed unnecessary to sample the time axis at a much higher resolution than the intrinsic dispersion on the TDE due to the presence of noise.

4.2 Deconvolution from a thin plate

In this section, results from NDT simulations are presented. A model of plane waves is used to describe the elastic propagation in layered materials [13]. This method enables to model compression and shear waves in anisotropic parts. The test piece is an aluminium plate immersed in water. The simulation aims to model the signal received by the transducer placed normally to the surface. The goal is to determine the thickness of the plate from an A-scan, by locating the echoes. The central frequency of the probe is 2.17 MHz, therefore the wavelength of longitudinal waves in aluminium is 2.92 mm. The sampling frequency imposed by the electronic system is 20 MHz. Figure 3 shows the pulse-echo wavelet for a normal incidence used for deconvolution (top panel) and the corresponding data for a 2 mm thick plate with

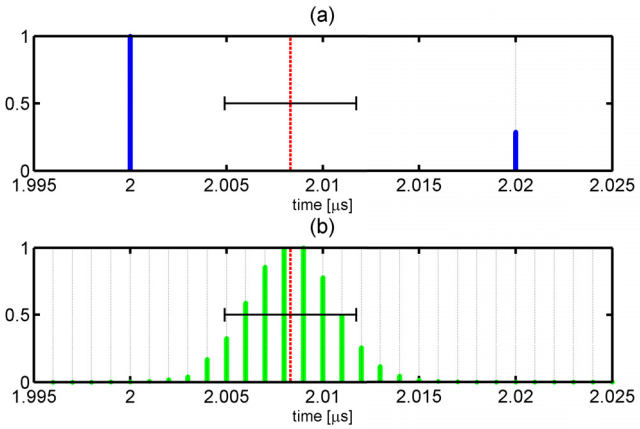

Figure 2: Histograms of time of flight estimation of a single echo (SNR = 0 dB). (a): DR, (b): SR with $K = 20$. True delay (dotted line), histograms of TDE (vertical bars). The error bar represents the standard deviation $\pm\sigma$ in Eq. (15). Dashed vertical lines refer to DR and SR discretisation grids.

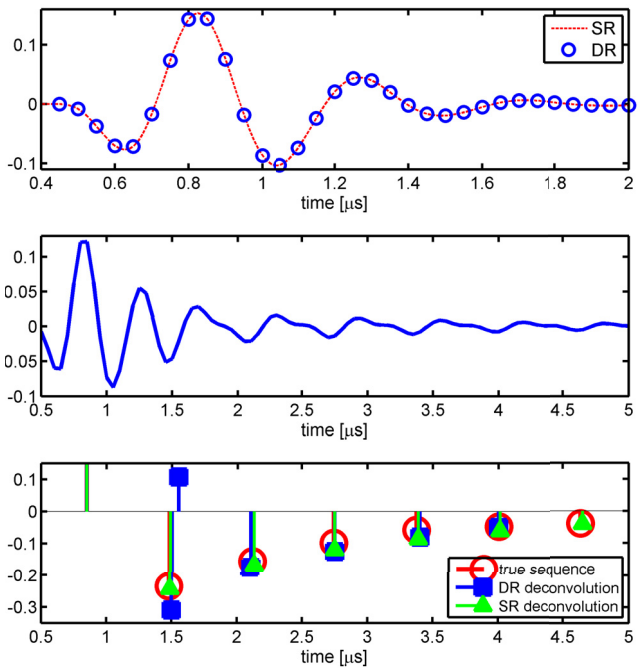

Figure 3: Deconvolution of an A-scan from an aluminium plate of thickness 2 mm with 30 dB SNR data. Top: DR and SR wavelets used for deconvolution (K=8). Centre: data. Bottom: results of DR and SR deconvolution.

30 dB SNR (centre panel). In this case, the thickness is less than the wavelength, leading to a prohibitive overlapping.

Deconvolution results are shown in the bottom panel. The surface echo, which has a large amplitude due to high impedance contrast between water and aluminium, is well identified by both methods at approximately 0.8 μs. Besides, the DR deconvolution creates double spikes for the second echo: since the restoration grid is not precise enough, the solution with only one spike does not fit well the data, so that the solution contains another close spike, with opposite amplitude, in order to compensate the error. SR deconvolution does not produce spike splitting thanks to the better precision of its sampling grid. It consequently returns a better location of the times of flight and can lead to a better thickness measurement. SR deconvolution hence gives acceptable results of amplitudes and times of flight, despite the difficulty of the problem.

Let us now examine the influence of the up-sampling factor K. Results of SR deconvolution, from the three first peaks, for $K = 2, 4$ and 8 are plotted in Figure 4. Results with $K = 2$ have obviously the worse time resolution. Furthermore, we can see that the precision is not increased from K equal 4 to 8. It is then useless to work at a higher up-sampling factor than 4. This limit is depending on the bandwidth of the transducer and the SNR, as we have seen in § 4.1.

4.3 Deconvolution from two close flaws

We consider here two overlapping echoes in the same conditions as in § 4.1. The simulations use DR and SR deconvolution to estimate the two times of flight (599 ns and 751 ns), which are not on the two restoration grids. This case simulates two close point flaws as described in Eq (3). Figure 5 shows the spike positions obtained by the SBR algorithm, against the parameter μ in Eq. (13). Globally, as μ increases, the number of spikes decreases, because of the growing importance of penalisation.

DR deconvolution does not give satisfactory results: solutions with only two or three detected spikes (for example, with $\mu = 10^{-1}$) show an important error on the spike locations. Indeed, the difference between the detected locations and the true ones is approximately half the frequency of the wavelet. Such solutions also yield a relatively low value of the data misfit term in criterion (13), but lead to strong confusion in the detection of the echoes. Solutions obtained for lower values of μ may detect the two spikes with better precision, but show a high number of artefacts.

On the contrary, SR deconvolution gives relevant solutions (*i.e.* two spikes), very close to the true solution, for a large range of μ ($10^{-1} \sim 10^{-3}$). It evidently reveals the interest of using a higher resolution rate. Such results illustrate the importance of using more precise discretisation in the data attachment model, especially for an L_0-based deconvolution approach with the SBR algorithm. Since L_0 optimisation only performs local optimisation, it is sensitive to local minima. Increasing the resolution then makes it easier for SBR to find better solutions.

5 Conclusion

A method of sparse deconvolution with a super-resolution approach was presented. Simulations with simple synthetic data revealed that this approach can improve the precision of the echo locations. Using a more precise model was also shown to improve the deconvolution results of the L_0-penalisation approach in the case of strongly overlapping echoes, whereas the usual formulation at the data resolution may lead to erroneous spike detections. In the context of layer localisation in non-destructive testing, we have shown from simulations that precision was increased by the super-resolution approach. Standard deconvolution creates double spikes when the true echoes are far from the restoration grid, whereas super-resolution estimation does not. Such improvements can be interpreted by considering that super resolution allows better data fitting, which favors the ability

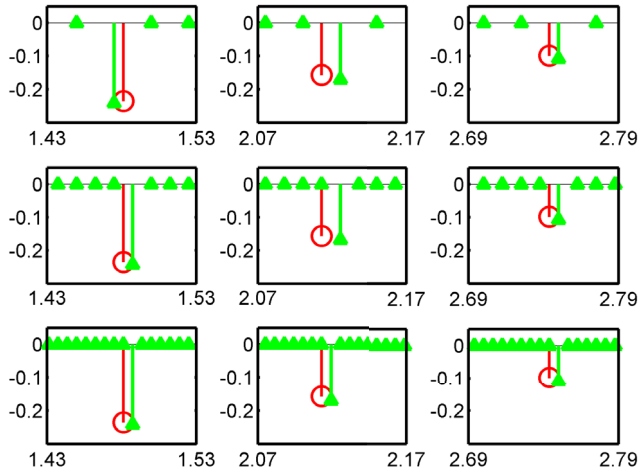

Figure 4: SR deconvolution from an aluminium plate of thickness 2 mm for different values of K. True ($\circ$) and estimated ($\triangle$) spikes. Top: $K = 2$, centre: $K = 4$, bottom: $K = 8$.

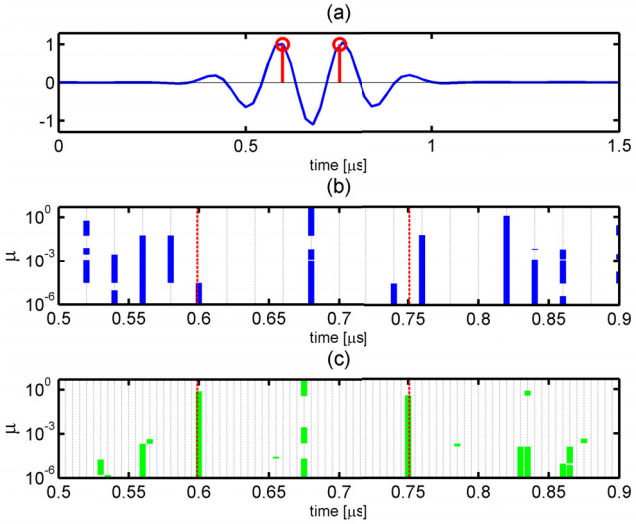

Figure 5: Estimation of times of flight against μ for two overlapping echoes. (a): data (full line) and true spikes ($\circ$). (b): DR deconvolution. (c): SR deconvolution with $K = 4$. True delays (dashed lines) and estimated locations (full lines). Dotted lines represent the restoration grids.

of the Single Best Replacement algorithm to retrieve satisfactory solutions. On the contrary, with lower resolution, such algorithm is more likely to fall into local minima of the objective function. We have seen that the up-sampling parameter of the super-resolution does not need to be too large since the restoration precision is limited by the presence of noise. This limit is actually related to the minimum variance of time delay estimation problems, which depends on the signal-to-noise ratio and on the transducer bandwidth. This point would deserve more attention in order to automatically tune the up-sampling parameter.

Acknowledgments

The authors wish to acknowledge Catherine Potel from the University of Maine, Le Mans, France, for providing the NDT simulation codes. This work has been partially supported by Region Pays de la Loire as part of the scientific program "Non-Destructive Testing and Evaluation Pays de la Loire" (ECND-PdL).

References

[1] J. Krautkramer, H. Krautkramer, *Ultrasonic Testing of materials*, Springer-Verlag Ed., (1990)

[2] M. Fink and J.F. Cardoso, "Diffraction effects in pulse-echo measurement", *IEEE Trans. on Sonics and Ultrasonics* **31**(4), 313-329 (1984)

[3] M.S. O'Brien, A.N. Sinclair and S.M. Kramer, "High resolution deconvolution using least-absolute-values minimization", *Ultrasonics Symposium, 1990. Proceedings.* **2**, 1151 -1156 (1990)

[4] S.K. Sin and C.H. Chen, "A comparison of deconvolution techniques for the ultrasonic nondestructive evaluation of materials", *IEEE Trans. on Image Processing*, **1**(1), 3-10, (1992)

[5] J. Idier, *Bayesian Approach to Inverse Problems*, ISTE Ltd and John Wiley & Sons Inc., (2008)

[6] D. Olofsson and T. Stepinski, "Maximum a posteriori deconvolution of ultrasonic signals using multiple transducers", *J. Acoust. Soc. Am.* **107**(6), 3276-3288 (2000)

[7] T. Cassereau, D. Guyomar and M. Fink, "Time deconvolution of diffraction effects - Application to calibration and prediction of transducer waveforms", *J. Acoust. Soc. Am.* **84**(3), 1073-1085 (1988)

[8] C. Soussen, J. Idier, D. Brie and J. Duan, "From Bernoulli-Gaussian Deconvolution to Sparse Signal Restoration", *IEEE Trans. on Signal Processing* **59**(10), 4572-4584 (2011)

[9] J. Duan, C. Soussen, D. Brie and J. Idier, "A continuation approach to estimate a solution path of mixed L2-L0 minimization problems", *SPARS Workshop* (2009)

[10] P. Stoica and Y. Selen, "Model-order selection: a review of information criterion rules", *IEEE Signal Processing Magazine* **21**(4), 36-47(2004)

[11] S. Bourguignon, C. Soussen, H. Carfantan and J. Idier, "Sparse deconvolution: Comparison of statistical and deterministic approaches", *IEEE Statistical Signal Processing Workshop (SSP)*, 317-320 (2011)

[12] A. Quazi, "An overview on the time delay estimate in active and passive systems for target localization", *IEEE Trans. on Acoustics, Speech and Signal Processing* **29**(3), 527-533 (1981)

[13] C. Potel and J.F. de Belleval, "Propagation in an anisotropic periodically multilayered medium", *J. Acoust. Soc. Am.* **93**(5), 2669-2677 (1993)